

REPORT DOCUMENTATION PAGE				Form Approved OMB No. 0704-0188	
<small>Public reporting burden for this collection of information is estimated to average 1 hour per response, including the time for reviewing instructions, searching existing data sources, gathering and maintaining the data needed, and completing and reviewing this collection of information. Send comments regarding this burden estimate or any other aspect of this collection of information, including suggestions for reducing this burden to Department of Defense, Washington Headquarters Services, Directorate for Information Operations and Reports (0704-0188), 1215 Jefferson Davis Highway, Suite 1204, Arlington, VA 22202-4302. Respondents should be aware that notwithstanding any other provision of law, no person shall be subject to any penalty for failing to comply with a collection of information if it does not display a currently valid OMB control number. PLEASE DO NOT RETURN YOUR FORM TO THE ABOVE ADDRESS.</small>					
1. REPORT DATE (DD-MM-YYYY)		2. REPORT TYPE Journal Article		3. DATES COVERED (From - To)	
4. TITLE AND SUBTITLE Comparison of Medium Power Hall Effect Thruster Ion Acceleration for Krypton and Xenon Propellants				5a. CONTRACT NUMBER	
				5b. GRANT NUMBER	
				5c. PROGRAM ELEMENT NUMBER	
6. AUTHOR(S) William A. Hargus, Jr.; Gregory M. Azarnia; Michael R. Nakles				5d. PROJECT NUMBER	
				5e. TASK NUMBER	
				5f. WORK UNIT NUMBER Q09W	
7. PERFORMING ORGANIZATION NAME(S) AND ADDRESS(ES) Air Force Research Laboratory (AFMC) AFRL/RQRS 1 Ara Drive Edwards AFB, CA 93524				8. PERFORMING ORGANIZATION REPORT NO.	
9. SPONSORING / MONITORING AGENCY NAME(S) AND ADDRESS(ES) Air Force Research Laboratory (AFMC) AFRL/RQR 5 Pollux Drive Edwards AFB, CA 93524				10. SPONSOR/MONITOR'S ACRONYM(S)	
				11. SPONSOR/MONITOR'S REPORT NUMBER(S) AFRL-RQ-ED-JA-2013-137	
12. DISTRIBUTION / AVAILABILITY STATEMENT Approved for public release; distribution is unlimited					
13. SUPPLEMENTARY NOTES Submitted for publication in Advances in Aircraft and Spacecraft Sciences PA Case Number: 13350; Clearance Date: 6/25/2013.					
14. ABSTRACT There is interest within the electric propulsion community in the use of krypton as a propellant for electrostatic thrusters. It is a lower cost replacement for xenon, may optimize to similar or potentially higher performance, and is enabling for very large solar electric transfer vehicles that would strain world-wide xenon production. This work compares the internal propellant acceleration of krypton ions within a laboratory medium power Hall effect thruster to xenon ion velocity data for the same thruster. One case matched in propellant particle flux, applied magnetic field, and accelerating potential is presented. The measurements consist of laser-induced fluorescence velocimetry extending from near the anode to 10 mm outside the thruster into plume along the center of the coaxial acceleration channel. This measurement region captures the majority of the propellant axial acceleration within the characterized 600 W medium power Hall effect thruster. The measurements show that krypton acceleration rate is lower and produces a lower effective electric field. As a result, energy conversion is lower than xenon for this flow matched case. In addition, there is clear evidence of krypton ionization throughout the acceleration channel, far downstream of where the majority of xenon acceleration occurs. This latent krypton ionization is consistent with the lower performance for krypton at this set of operating conditions due to low propellant utilization.					
15. SUBJECT TERMS					
16. SECURITY CLASSIFICATION OF:			17. LIMITATION OF ABSTRACT	18. NUMBER OF PAGES	19a. NAME OF RESPONSIBLE PERSON
a. REPORT	b. ABSTRACT	c. THIS PAGE			William A. Hargus, Jr.
Unclassified	Unclassified	Unclassified	SAR	12	19b. TELEPHONE NO (include area code) N/A

Comparison of Medium Power Hall Effect Thruster Ion Acceleration for Krypton and Xenon Propellants

William A. Hargus, Jr.*

Gregory M. Azarnia†

Michael R. Nakles‡

Air Force Research Laboratory, Edwards Air Force Base, CA 93524

There is interest within the electric propulsion community in the use of krypton as a propellant for electrostatic thrusters. It is a lower cost replacement for xenon, may optimize to similar or potentially higher performance, and is enabling for very large solar electric transfer vehicles that would strain world-wide xenon production. This work compares the internal propellant acceleration of krypton ions within a laboratory medium power Hall effect thruster to xenon ion velocity data for the same thruster. One case matched in propellant particle flux, applied magnetic field, and accelerating potential is presented. The measurements consist of laser-induced fluorescence velocimetry extending from near the anode to 10 mm outside the thruster into plume along the center of the coaxial acceleration channel. This measurement region captures the majority of the propellant axial acceleration within the characterized 600 W medium power Hall effect thruster. The measurements show that krypton acceleration rate is lower and produces a lower effective electric field. As a result, energy conversion is lower than xenon for this flow matched case. In addition, there is clear evidence of krypton ionization throughout the acceleration channel, far downstream of where the majority of xenon acceleration occurs. This latent krypton ionization is consistent with the lower performance for krypton at this set of operating conditions due to low propellant utilization.

Introduction

At present, xenon (Xe) is the propellant of choice for most electrostatic plasma thrusters including Hall effect thrusters. The selection of xenon is due to a number of rigorous engineering rationale. These include the high mass (131 amu) and relatively low ionization potential (12.1 eV) of xenon; as well as the inert nature of xenon, which eliminated much of the controversy that plagued early electrostatic propulsion efforts when mercury (Hg) and cesium (Cs) were the propellants of choice.¹ Although xenon is a noble gas, it is the most massive, and due to its non-ideal gas behavior, it is possible to pressurize and store with room temperature specific densities approaching 1.6.^{2,3} As such, it may be stored at higher densities than that of the most common liquid monopropellant, hydrazine, which as a specific gravity of approximately 1.

While xenon remains an ideal propellant for electrostatic thrusters such as Hall effect thrusters, there are several concerns that drive the Hall effect thruster community to explore alternative propellants. As orbit raising missions of longer duration and larger payloads are proposed, requisite propellant mass increases dramatically. Xenon production is a byproduct of the

fractional distillation of atmospheric gases for use primarily by the steel industry. Due to the low concentration of xenon in the atmosphere (~90 ppb), worldwide production is only approximately 6,000 standard cubic meters (35×10^3 kg) per year. Increasing industrial demand for items such as high efficiency lighting and windows, as well as plasma based micro-fabrication, has produced wide price swings in the past decade. Xenon prices have varied by as much as factor of ten in the past five years alone.

For missions that benefit from higher specific impulse, krypton (Kr) propellant has benefits beyond its lower cost. Krypton has a lower atomic mass (83.8 amu), but a slightly higher ionization potential (14.0 eV) than xenon. Like xenon, krypton is a noble gas and could be easily integrated into existing Hall effect thruster propellant management systems without significant modification. The similar ionization potential should not dramatically affect Hall effect thruster efficiency, and the lower atomic mass should produce a 25% increase in specific impulse. The increase in specific impulse may be useful for missions such as station-keeping where increased specific impulse is advantageous. For missions such as orbit raising, increasing the specific impulse may increase trip time due to power limitations. Still, as solar electric power generation system specific power decreases, increasing the specific impulse of

*Senior Engineer, AFRL/RQRS, Edwards AFB, CA, USA.

†Physicist, ERC, Inc., Edwards AFB, CA, USA.

‡Senior Engineer, ERC, Inc, Edwards AFB, CA, USA.

Table 1 Comparison of xenon and krypton properties critical for electrostatic propulsion.²

Property	Units	Xe	Kr
Atomic Mass	amu	131.3	83.8
1 st Ionization Energy	eV	12.1	14.0
2 nd Ionization Energy	eV	21	24
3 rd Ionization Energy	eV	32	37
Atmospheric Concentration	ppb	87	1000
Stable Isotopes		9	6
Odd Isotopes		2	1
Critical Pressure	MPa	5.84	5.50
Critical Temperature	K	290	209
Boiling Point (1 atm)	K	161	120

the propulsion system can maintain trip time while reducing total system mass. Krypton is approximately $10\times$ more common in the atmosphere (and hence in production) than xenon, and when accounting for mass is approximately $6\times$ less expensive. Table 1 summarizes the relevant properties of xenon and krypton.²

In order to assess whether the potential advantages of krypton propellant can be realized in Hall effect thrusters and other electrostatic thruster types, experimental measurements of these plasmas are required; both to determine relative figures of functional merit and for numerical simulation validation for increased fundamental understanding of subtle propellant effects. This effort's goal is to begin the comparison of krypton and xenon acceleration in the same thruster under comparable conditions. For one case of matched propellant particle flux (atoms/second), this work compares the internal propellant acceleration of krypton within a laboratory medium power (600 W) Hall effect thruster to xenon measurements for the same thruster. The single case with matched applied magnetic field, acceleration potential, and volumetric flow does not optimize for propellant characteristics. The conditions chosen were based on known optimized xenon conditions. The comparison is valuable for both measuring the impacts of subtle changes in propellant as well as for validation of numerical models simulating these thrusters and fundamentally understanding that impact.

Laser-Induced Fluorescence

Laser-induced fluorescence (LIF) may be used to detect velocity-induced shifts in the spectral absorption of various plasma species with high spatial resolution. The fluorescence is monitored as a continuous-wave laser is tuned over the transition of interest, of energy $h\nu_{12}$; where h is Planck's constant, ν_{12} is wavenumber of transition between lower state 1 and higher energy state 2. Note that state 1 may be the ground state, but any sufficiently highly populated excited state will

do. For the highly excited, but low density accelerated plasmas of interest, we generally choose to examine a metastable state to ensure high signal levels at convenient excitation wavelengths. Measurements can be made with high spatial resolution as determined by the intersection of probe laser beam with fluorescence optical collection.

Velocity measurements are made using LIF velocimetry as an ion population moving with a velocity component u relative to the direction of the incoming laser absorbs photons at a frequency shifted from that of stationary absorbers due to the Doppler effect. The magnitude of this frequency shift $\delta\nu_{12}$ is

$$\delta\nu_{12} = \frac{u}{c}\nu_{12}. \quad (1)$$

The measured fluorescence lineshape is determined by the environment of the absorbing ion population, so an accurate measurement of the lineshape function may lead to the determination of a number of plasma parameters beyond simple bulk velocities. The precision of measured velocities has been found, in various studies, to be less than the experimental uncertainty for the ions (± 500 m/s).^{4,5,6}

LIF is a convenient diagnostic for the investigation of ion velocity distributions in a plasma as it does not physically perturb the discharge. The fluorescence signal is a convolution of the velocity distribution function (VDF), transition lineshape, and laser beam frequency profile. Determination of the VDF from LIF data only requires the deconvolution of the transition lineshape and laser beam profile from the raw LIF signal trace. Alternatively, the lineshape itself may also provide valuable information on the state of the plasma, such as electron density, pressure, or heavy species temperature. In the somewhat turbulent plasmas typical of Hall effect thrusters, the fluorescence lineshape can also be indicative of the relative motion of the ionization zone as it axially traverses in the periodic breathing mode plasma fluctuation.^{7,8} However, care must be taken to ensure that the relative effects of these phenomena are separable. In addition, magnetic (Zeeman effect) and electric (Stark effect) fields may also influence the fluorescence lineshape⁹ and must be accounted for when analyzing the lineshapes should the fields be of sufficient magnitude. In the case of LIF of ions in a Hall effect thruster, the fluorescence lineshape appears to be most indicative of the aforementioned plasma turbulence including periodicity in the positions of the ionization zone within the acceleration channel.

We have examined the spectroscopy of the krypton ions and have recently developed LIF measurement capabilities with regard to the 728.98 nm $5d^4D_{7/2}-5p^4P_{5/2}^o$ Kr II transition. The details of application of Kr II LIF using the metastable $5d^4D_{7/2}$ state and exciting to the $5p^4P_{5/2}^o$ state using a laser at 728.98 nm

Table 2 *Nominal thruster operating conditions.*

	Kr	Xe
Anode Flow	25.5 sccm 1.59 mg/s	25.5 sccm 2.45 mg/s
Cathode Flow	1.5 sccm 94 μ g/s	1.5 sccm 147 μ g/s
Anode Potential	300 V	300 V
Anode Current	1.73 A	1.93 A
Inner Coil Current	1.75 A	1.75 A
Outer Coil Current	1.75 A	1.75 A
Keeper Current	0.5 A	0.5 A
Heater Current	3.0 A	3.0 A
Measured Thrust	22.4 mN	35.8 mN
Anode Efficiency	31%	44%
Specific Impulse	1440 s	1460 s

are detailed elsewhere.^{11,12} This new capability complements our previously developed Xe II LIF capabilities.^{13,14}

Apparatus

Vacuum Facility and Thruster

All LIF measurements were performed in Chamber 6 of the Air Force Research Laboratory (AFRL) Electric Propulsion Laboratory at Edwards AFB, CA. Chamber 6 is a non-magnetic stainless steel chamber with a 1.8 m diameter and 3 m length. Pumping is provided by four single-stage cryogenic panels (single-stage cold heads at 25 K) and one 50 cm two stage cryogenic pump (12 K). This vacuum test chamber has a measured pumping speed of 36 kL/s on xenon.

The Hall thruster used in this study is a medium power laboratory Hall effect thruster manufactured by the Busek Company of Natick, MA, USA, which has been described in detail elsewhere.¹⁴ This thruster is designed for operation on xenon and performance has only been characterized for krypton for limited operating conditions, although extensive plume measurements are available.¹⁵ Thruster operation for this effort consisted of a single stable condition shown on Table 2. Unpublished thrust measurements from our laboratory show krypton operation of the BHT-600 at the conditions in Table 2 yields a thrust of 22.4 mN corresponding to an anode efficiency of approximately 31%. Since this thruster at the conditions at which measurements were taken is optimized for xenon, performance with xenon propellant is much superior compared to krypton. The single operating condition serves as a direct comparison of the differences between xenon and krypton without the complexity of interpreting the optimization of applied magnetic field and acceleration potential.

Vacuum chamber background pressure during thruster operation was measured with a cold cathode ionization gauge and is approximately 3×10^{-3} Pa, corrected for krypton (using an N₂ conversion to Kr

multiplicative factor of 0.59), and for the xenon case, the background pressure was 2×10^{-3} Pa, corrected for xenon (using an N₂ conversion to Xe multiplicative factor of 0.67).¹⁶ Due to the use of a cold cathode ionization gauge, the background pressure uncertainty is estimated to be greater than 30%. During thruster operation, the thruster parameters shown in Table 2 are monitored and recorded at a 0.2 Hz data rate.

Laser and Optics

The laser used for Kr II LIF is a custom built ± 50 GHz tunable diode laser (Newport Optics, New Focus Division) centered on the $5d^4D_{7/2}-5p^4P_{5/2}^o$ transition at 728.98 nm. It is a Littman-Metcalf external cavity tunable diode laser capable of mode hop free tuning across its 100 GHz tuning range at output powers as high as 25 mW with a line width of less than 500 kHz.

Based on previous efforts,¹³ the laser, probe beam launch optics, and fluorescence collection optics are located on two optical tables placed about viewports with optical access into the vacuum chamber as shown in Fig. 1. On the primary optics table, the diode laser beam first passes through a Faraday isolator to eliminate laser feedback. The laser beam then passes through a 10% wedged beam pick-off (PO) to provide beam diagnostics. The first of the two reflections (each approximately 5% of incident power) is directed onto a photodiode detector (D1) and provides constant power feedback to the laser. The second pick-off beam passes through a 300 MHz free spectral range, high finesse Fabry-Perot etalon (F-P) that provides frequency monitoring of the wavelength interval swept during a laser scan.

The main laser beam is then chopped at 3 kHz by a mechanical optical chopper for phase sensitive detection. It is then divided into two equal components by a 50:50 cube beam splitter (BS). The first component passes through a krypton opto-galvanic cell and is terminated by a beam dump. The opto-galvanic cell current is capacitively coupled to a lock-in amplifier in order to monitor the Kr II 728.98 nm $5d^4D_{7/2}-5p^4P_{5/2}^o$ transition to provide a zero velocity reference.¹⁷

The probe beam is then directed via several mirrors and focused by a single lens to a sub-millimeter beam waist within the chamber vacuum through a glass vacuum viewport. The fluorescence collection optics, also shown in Fig. 1, collect the signal generated at the beam waist. The fluorescence is collected by a 75 mm diameter, 300 mm focal length lens within the chamber. The collimated signal is directed through a window in the chamber side wall to a similar lens that focuses the collected fluorescence onto the entrance slit of 125 mm focal length monochromator with a photomultiplier tube (PMT) detector. The PMT signal is then analyzed using a second lock-in amplifier. The spatial resolution of the measurements is determined

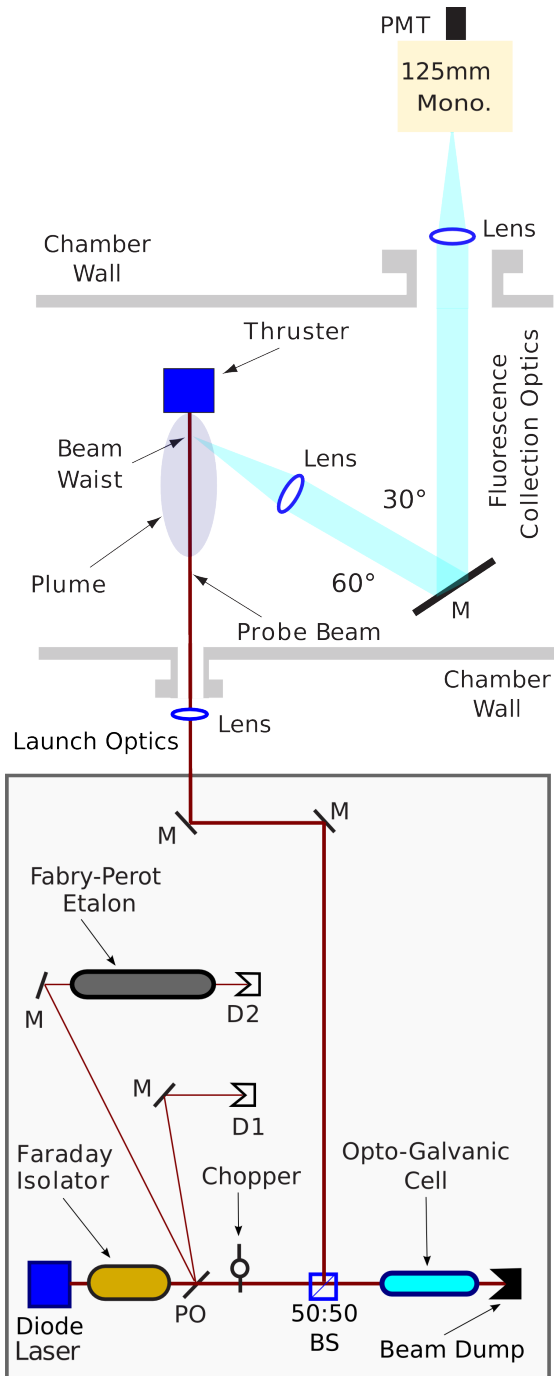


Fig. 1 Layout of Kr II laser-induced fluorescence apparatus showing all relevant optical components, portions of the vacuum chamber, and Hall effect thruster plume.

by the geometry of the spectrometer entrance slit (note the 1:1 magnification of the collection optics).

The Xe II LIF measurements use a nearly identical experimental apparatus with a different diode laser. For the xenon results reported here, the $5d[4]_{7/2} - 6p[3]_{5/2}$ electronic transition of Xe II at 834.72 nm is probed with a 15 mW maximum power Littman-Metcalf external cavity tunable diode laser

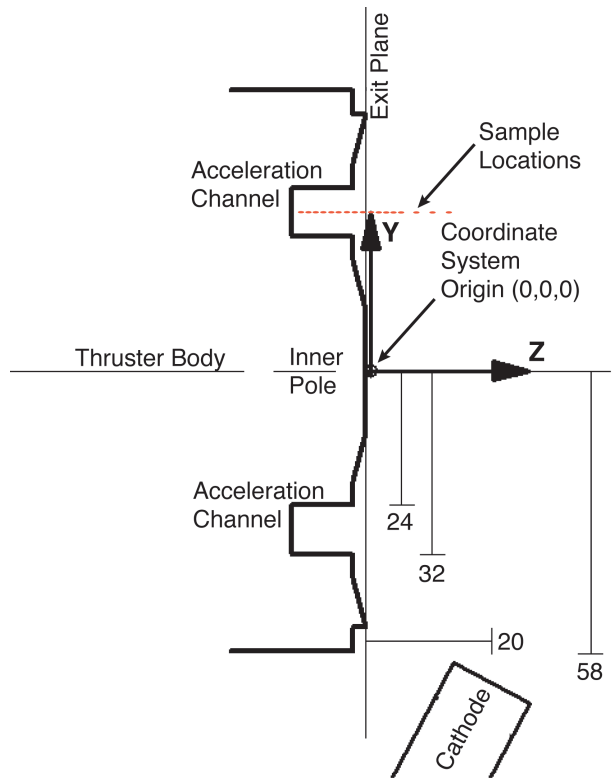


Fig. 2 Cutaway view of the BHT-600 Hall effect thruster with measurement volume shown in red.

capable of mode hop free tuning across approximately 80 GHz tuning range. The isotopic and nuclear-spin effects contributing to the hyperfine structure of the $5d[4]_{7/2} - 6p[3]_{5/2}$ xenon ion transition produce a total of 19 isotopic and spin split components. The hyperfine splitting constants that characterize the variations in state energies are only known for a limited set of energy levels. Unfortunately, the 834.7 nm xenon ion transition only has confirmed data on the nuclear spin splitting constants of the $6p[3]_{5/2}$ upper state.^{4,18,19,20} Manzella first used this $5d[4]_{7/2} - 6p[3]_{5/2}$ xenon ion transition at 834.7 nm to make velocity measurements in a Hall thruster plume.²¹ A convenient feature of this transition is the presence of a relatively strong line originating from the same upper state ($6s[2]_{3/2} - 6p[3]_{5/2}$ transition at 541.9 nm,²² which allows for non-resonant fluorescence collection). Ion velocity is simply determined by measurement of the Doppler shift of the absorbing ions. As a stationary reference, there is a nearby (measured to be 18.1 GHz distant) neutral xenon $6s'[1/2]_1 - 6p'[3/2]_2$ transition at 834.68 nm.^{23,24} The xenon results are reported separately elsewhere in greater detail by Nakles and Hargus.¹⁴

LIF Velocity Measurements

Measurement Domain

Figure 2 shows a cross-section of the BHT-600 Hall effect thruster used in this test. Annotated in red

is the measurement volume. The volume consists of a linear set of data points spaced by 1 or 2 mm at $X=0$, $Y=28$ mm with Z varying between -9 mm and +12 mm. Note that $Z=0$ denotes the geometrical exit plane of the thruster.

Velocity Distributions

Raw fluorescence traces are a reasonable representation of the ion velocity distribution (VDF) so long as the lineshape width is small compared to the velocity distribution. Recall that the fluorescence traces measured are the convolution of the true VDF, the transition lineshape, and the laser line width. The transition lineshape has been modeled and found to be relatively narrow compared to the fluorescence trace.^{11,25} In turn, the laser line widths are only approximately 500 kHz. As a result, the fluorescence lineshape magnitude is within 10–15% of the time averaged VDF. This is consistent with previous velocity distribution measurements for xenon that showed that deconvolution of the transition lineshape was not necessary in the near plume.²⁶

Figure 3 shows the evolution of the velocity distributions of krypton ions. Nearest the anode, the VDF at $Z = -8$ mm shows a slight negative velocity. This is either indicative of the small uncertainties in the measurements, or may alternatively be a manifestation of the ion drag toward the anode by the electron current. These negative velocities are consistent with previous measurements of xenon Hall effect thrusters.^{4,7,8,14}

Prior to $Z = -4$ mm, we interpret the krypton ion velocity distributions as indicative of a single velocity population; all of which were created at approximately the same plasma potential and that activity in this region is dominated by ionization with little acceleration. By $Z = -4$ mm we see that a portion of the velocity distribution has been accelerated to a velocity around 4 km/s, and as high as 8 km/s. However, there is evidence of significant ionization yet occurring as 20–30% of the population has velocities of less than 3 km. Interestingly, we see significant low velocity krypton ion populations from this axial position forward into the plume showing low velocity ion population components. This implies that significant ionization is occurring at all measurement locations, including those in the outside the thruster.

Figure 4 shows an equivalent to Fig. 3 of the xenon ion velocity distributions. The complete data taken from velocity distributions measured by Nakles and Hargus¹⁴ is shown in Fig. 5, where the much broader peaks of the xenon case are more clearly separated. The xenon velocity distributions in Fig. 5 have substantial differences when compared to the krypton ion velocity distributions in Fig. 3. First, the xenon velocity distributions are significantly broader. This appears to be a function of the oscillatory behavior of the anode discharge and is quantified by Nakles and

Hargus, as due to thruster *breathing mode* where an axial ionization wave first forms near the anode and then travels out into the plume. In the plume, the ionization wave dissipates due to a lack of neutrals for ionization, whereupon it reforms near the anode once more. This is a typical behavior of Hall effect thrusters and usually occurs with frequencies of a few to several tens of kHz.²⁷

At the operating condition examined in this work, xenon exhibits a strong breathing mode oscillation that dominates the anode current. On the other hand, krypton is very much quiescent and the breathing mode here manifests itself as a small current ripple on the generally DC anode current. It is believed that the breathing mode oscillations enhance electron transport since although the ionization wave ultimately travels outward in the axial direction, it is also composed of a series of azimuthal instabilities that promote turbulent cross-field electron transport also known as Bohm diffusion, or so called *anomalous diffusion*.²⁸ As a result, the xenon velocity distributions are much broader as the electron cross-field transport enhancing ionization wave traverses the acceleration channel and dissipates somewhere in the near plume, all the while broadening the plasma acceleration in velocity space. Evidence of this is shown in Fig. 5 starting at $Z = -4$ mm where we have evidence of ionization (zero velocity ions) and a high velocity tail extending approximately 12 km/s, much higher than the most probable velocity of 4 km/s. There is no equivalent behavior in the krypton velocity distributions of Fig. 3.

Another difference between the two propellants is the significant proportion of low velocity krypton ions and evidence of ionization occurring throughout the acceleration channel and into the plume. For example, at $Z = +12$ mm, the krypton velocity distribution in Fig. 3 is 35–40% in the low velocity region (defined as below 18 km/s), where the most probable velocity is 22.4 km/s and the resulting mean velocity of the distribution is 16.8 km/s. It bears consideration that for krypton, while 35–40% of the ions are in the low velocity region, this region only contains 15% of the velocity distribution's energy. In contrast, the xenon case appears to have only a very small amount of late ionization, such that it cannot be distinguished from the background.

Despite the obvious differences in the velocity distributions shown in Figs. 3 and 4, the general behavior remains remarkably similar. The initially narrow velocity distributions, where primarily only ionization is occurring, are broadened in the region of the discharge where ions are both being created and ionized. Starting in the region defined by the geometrical exit plane and extending into the near plume, the velocity distributions narrow by kinematic compression as the ionization rate drops and the entire ion population is accelerated further.

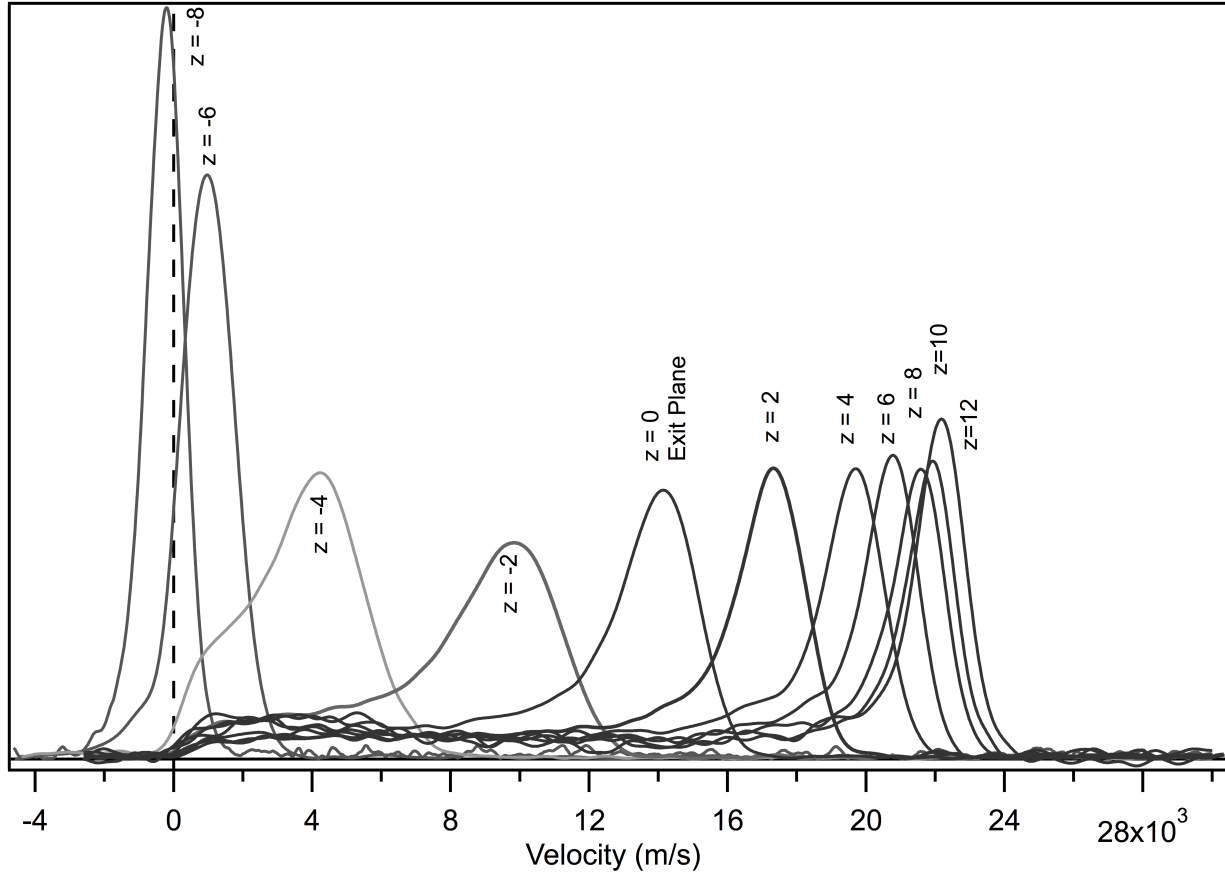


Fig. 3 Velocity distributions of krypton ions showing acceleration of the propellant stream from $Z = -8$ mm to $Z = +12$ mm. Note that each distribution is individually normalized to unity area.

Comparing the values of Table 2 between xenon and krypton provides some insights of global measurements (e.g. propellant utilization) in conjunction with the LIF measurements. First, due to the higher atomic mass of xenon (131.3 vs 83.8 amu), the delivered thrust is significantly higher for xenon (35.8 vs 22.4 mN). But as noted earlier, it is important to note that the volumetric flow rates (atom flux, or atoms/second) are equal for both xenon and krypton cases discussed here. Interestingly, thruster efficiency is significantly lower for the krypton case than for xenon, and the specific impulse values are approximately the same. Based on atomic mass alone, and assuming equivalent ionization, one would expect the specific impulse of krypton to be 125% that of xenon. The combination of lower energy conversion efficiency and equivalent specific impulse indicate a lower propellant utilization fraction for krypton as is indicated by the persistent late term ionization in Fig. 3.

Most Probable Velocity

Figure 6 shows the most probable velocities measured for both krypton and xenon. The most probable velocities correspond to the peak of the extracted fluorescence curves shown in Figs. 3 and 5. While a

much more limited comparison of the velocity measurement than the comparison of the VDFs, the most probable velocity is valuable since it provides a singular value that characterizes the behavior of the peak of the velocity distribution. The most probable velocity obviously differs from the mean and median velocity values; however, we feel that use of this value provides a valid comparison so long as the distribution is not particularly broad and the fluorescence has adequate signal to noise ratios (SNR).

It should be noted that the most probable velocity is easily extracted with minimum ambiguity from noisy data, if the distribution is somewhat regular. The mean of a noisy velocity distribution contains substantially greater uncertainty since the baseline and extent of the distribution is difficult to determine without introducing experimental bias. As such, the most probable velocity remains a useful tool for comparisons of velocity evolution profiles such as those in this study. The most probable velocity becomes ambiguous if there are multiple peaks, which often occurs further in the plume where there may be multiple populations of ions interacting.¹² This can also occur within the thruster as clearly shown in Figs. 3 and 4, where there are distinct regions of ion creation overlapped with ion

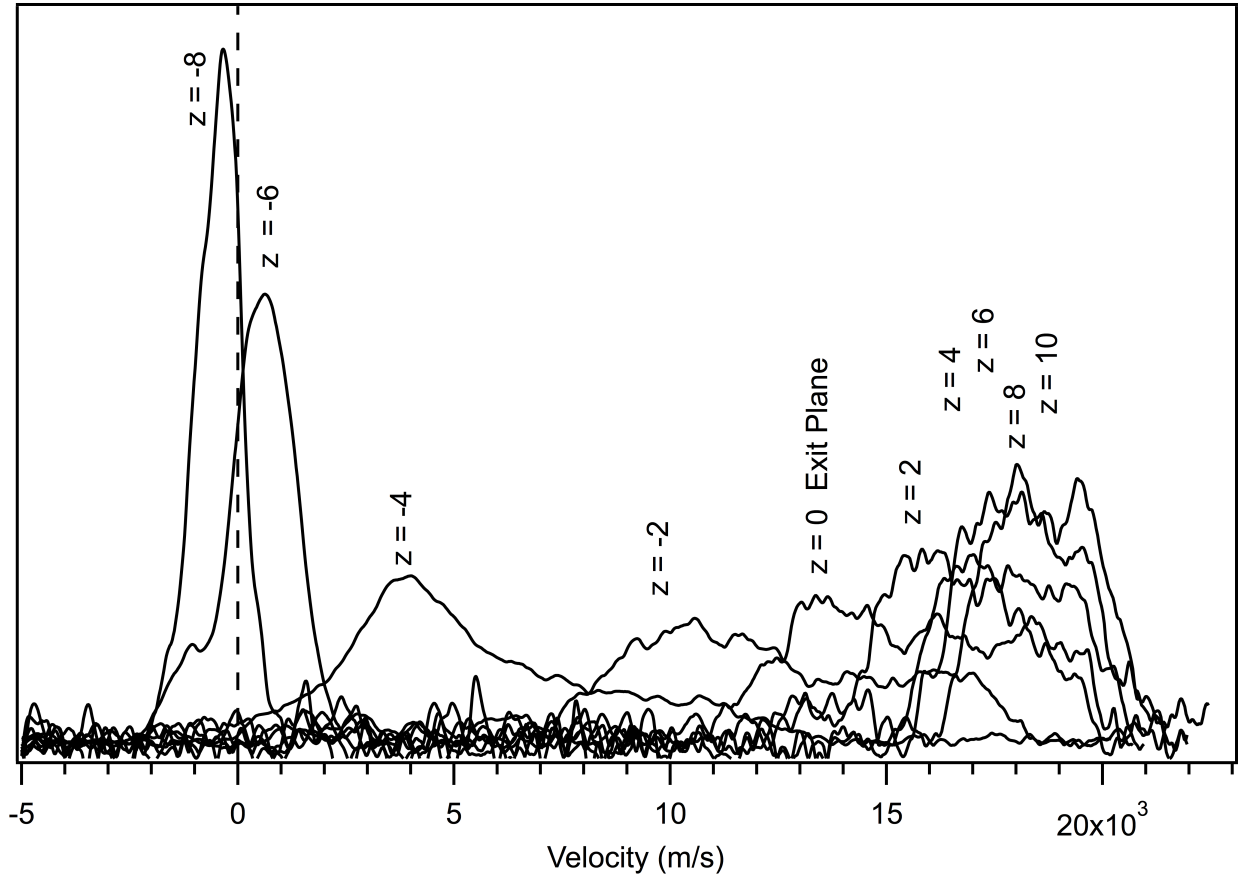


Fig. 4 Velocity distributions of xenon ions showing acceleration of the propellant stream from $Z = -9$ mm to $Z = +10$ mm. Note that each distribution is individually normalized to unity area.

acceleration regions.

The velocity profile in Fig. 6 shows the velocities slightly negative, nearest the anode (at approximately -9 mm). This negative velocity near the anode may be attributed to the anode sheath producing a small acceleration potential toward the anode for ions as a result of the anode electron flow. Interestingly, this ion velocity behavior has been measured in a similar plasma accelerator previously, where the neutrals also exhibit a negative velocity near the anode, presumably due to ion drag.⁴

Further from the anode, the most probable velocity of both krypton and xenon climbs smoothly, showing maximum acceleration near, but within the thruster geometric exit plane ($Z=0$). The peak krypton ion velocity is just below 24 km/s at $Z = +12$ mm and is presumed to rise steadily beyond the measurement region. The xenon most probable ion velocity follows within about 1–2 km/s of the krypton velocity until near the exit plane. Here, the xenon ion acceleration slows substantially. While the krypton ion acceleration decreases here as well, krypton ion acceleration continues at a higher rate than for xenon. At the furthest extent of matching measurements, krypton ion velocities are approximately 17% higher than those of

xenon.

Energy Deposition

An effective illustration of energy deposition into the propellant from the plasma discharge is to calculate the profile of measured ion kinetic energy. We chose to make this calculation using the most probable velocities shown in Fig. 6. Calculating the kinetic energies of the propellant using $\frac{1}{2}mv^2$ and expressing the units in eV, we arrive at Fig. 7.

Figure 7 compares the energy deposition of the xenon and krypton propellants. The general behavior is very similar, but the krypton energy deposition is consistently lower than that of xenon. Although the acceleration begins in the same region, the rate of acceleration is lower for krypton. The divergence in propellant energy deposition between krypton and xenon occurs throughout the measurement region.

In Fig. 7, we see that substantial energy deposition into the propellant does not begin until approximately $Z = -4$ mm. The calculated kinetic energies also more clearly show that there is substantial energy deposition occurring beyond the exit plane. This confirms that propellant acceleration extends into the near plume region, and further than the spatial extent of the mea-

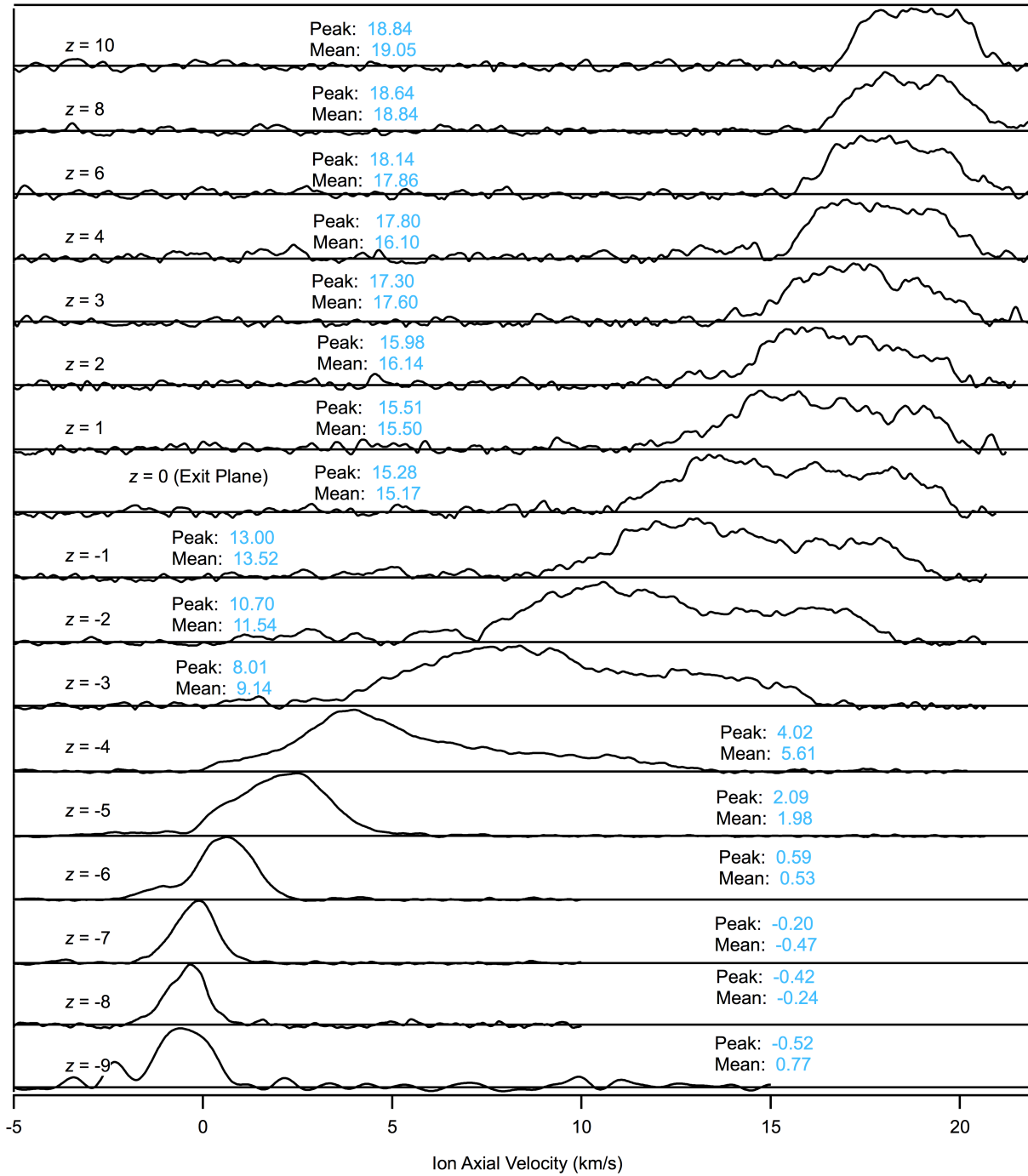


Fig. 5 Xenon velocity distributions shown individually.¹⁴ Peak (most probable) and mean (population weighted) velocities are given for each velocity distribution in km/s.¹⁴

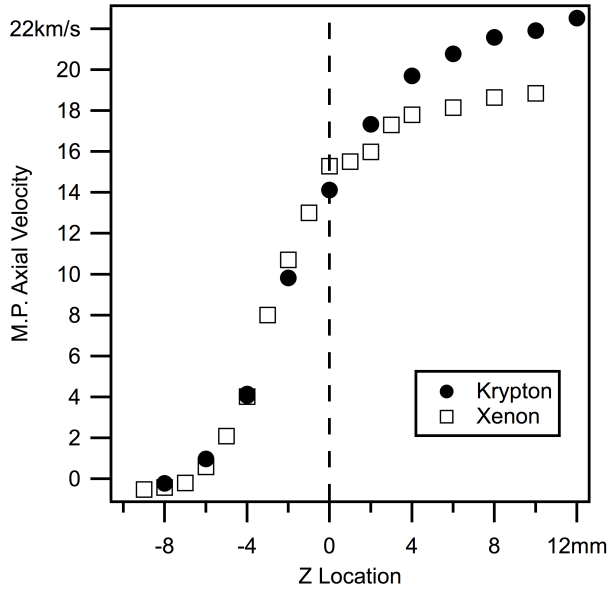


Fig. 6 Most probable krypton and xenon velocities of the BHT-600 Hall effect thruster. Note that $Z=0$ denotes the location of the exit plane.

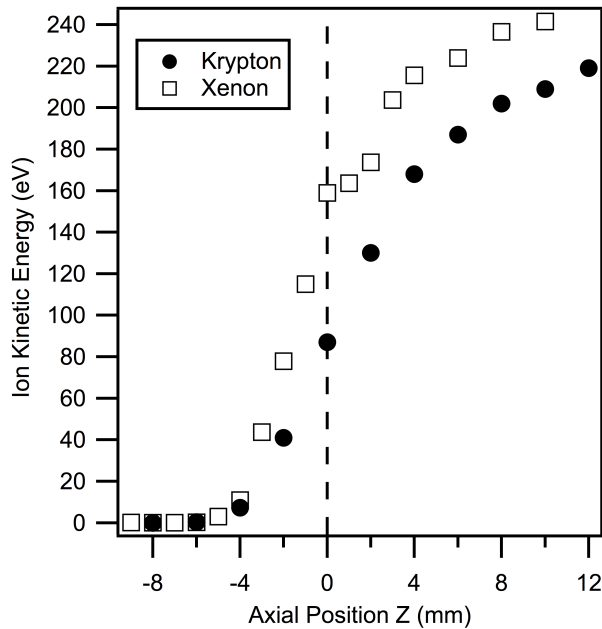


Fig. 7 Comparison of krypton and ion kinetic energies calculated from most probable ion velocities.

measurements. The peak ion energy for xenon is approximately 240 eV and approximately 220 eV for krypton. This is lower than the 300 V applied discharge potential, indicating that not all the applied potential is recovered by the propellant.

An electric field axial component E_z may be calculated from the derivative of the kinetic energies using the relationship $E_z = -\nabla_z \phi$. This *effective* electric field is calculated by taking the ion kinetic energies

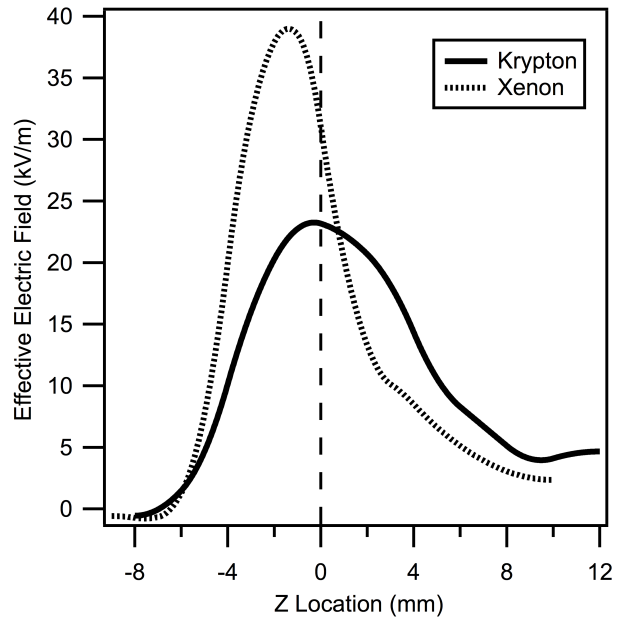


Fig. 8 Comparison of krypton and xenon effective axial electric fields acting on accelerated ions calculated using most probable kinetic energies.

in Fig. 7 and fitting a smoothing spline that is subsequently numerically differentiated. The resultant electric field is believed to be an adequate measure of the effective electric field acting on the ions. The use of the most probable velocity at the root of this calculation lessens ambiguity and provides maximum repeatability, but most likely is not a true representation of the electric field, which has considerably more complexity in both the spatial and temporal domains. With that caution, the effective electric field calculated here is the only such non-intrusive measurement available.

Figure 8 shows the calculated axial electric field within the thruster and extending into the near plume. For krypton, the effective electric field peaks at 23 kV/m just inside the thruster exit plane near $Z=0$. A significant portion of the electric field is outside the thruster. The magnitude of the krypton electric field is approximately 4 kV/m at $Z = +12$, which may be an edge effect, or an artifact of the limited number of measurements. The electric field calculated for xenon peaks at approximately 39 kV/m, a value 60% higher than krypton. The peak field for xenon is further with the thruster peaking at approximately $Z = -2$ mm.

In comparison to the effective electric field calculated for xenon, we see that the krypton effective electric field peaks at a substantially lower magnitude and further downstream, closer to the exit plane than for xenon. The effective electric fields are not similar in shape as that of krypton is substantially wider and less peaked. The reason for this difference is not fully understood. There are a number of contributing factors that may in some combination explain this

difference in electric field profile. First, as the drift velocity of the neutrals is inversely proportional with atomic mass, the krypton neutrals are likely to travel further out of the thruster channel than the xenon neutrals prior to ionization. As a result, the krypton neutrals have a higher probability of exiting the channel without ionization and being lost to electrostatic acceleration. The slightly higher ionization energy of krypton also contributes to this effect. This is consistent with the krypton effective electric field's larger magnitude outside the thruster in Fig. 8, and by late krypton ionization occurring throughout the measurement region in Fig. 3. Second, the lower magnitude breathing mode oscillations of krypton likely promotes lower electric fields simply due to the lessening of turbulent transport. As a result, the electric potential fall would have a larger spatial extent for krypton. There may also be an effect related to the higher acceleration of krypton (related to the 25% lower atomic mass) reducing the plasma density and thereby reducing transport across magnetic field lines.

The relative importance of these mechanisms, or other unidentified mechanisms, is not fully understood. However, there are some thruster design implications for krypton. A longer channel length that provides a longer residence time may be necessary for more complete ionization of krypton propellant. Increased axial extent would also better encompass the greater distribution of the effective electric field. Raising the acceleration potential may also result in higher electron temperature in the ionization region of the discharge. The higher electron temperature may overcome the higher krypton ionization potential relative to xenon. Increasing the density of the discharge by increasing the krypton volumetric flow rate (atoms/second) would also increase plasma density and thereby increase the likelihood of ionization events. However, increasing the accelerating potential would also decrease the plasma density due to acceleration. So some of these potential methods by which krypton thruster performance may be increased require careful optimization.

Other studies in the optimization of krypton propellant in Hall effect thrusters have shown that improved thruster design for krypton is achievable.^{29,30,31} However, parameter optimization appears to require substantial experimental verification. The results of these parallel studies have much in common with the results of this work. The LIF verifies many of the hypotheses made to explain the differences due to xenon and krypton properties. Future efforts must examine optimized krypton cases so that performance differences as a result of propellant selection can be more fully understood.

Discussion and Conclusions

Comparison of xenon and krypton for a single thruster operating parameter where the atomic flow rate, applied acceleration potential, and applied radial magnetic field are all equal demonstrated that simple changes in propellant result in dramatic changes in the acceleration of the propellant both within and in the near plume of a medium power Hall effect thruster. We chose to examine a nominal xenon case with a krypton case with the same applied parameters. As a result the Hall effect thruster designed and optimized for xenon performed significantly worse for krypton. The LIF diagnostic allowed us to identify energy deposition and propellant utilization as the primary culprits for this particular set of operating parameters.

The differences between krypton and xenon for this single matched case illuminate fundamental differences in the behavior of these propellants with an otherwise identical applied acceleration potential and electron retarding magnetic field. For example, the most probable ion velocities are about 15% higher for krypton with a resultant lower plasma density. Electron cross-field transport is almost certainly affected by the significantly lower breathing mode of krypton. Also consider that the ionization potential of krypton is 16% higher than that of xenon and as a result krypton has a lower electron collision ionization cross-section. The lower mass of krypton relative to xenon also reduces neutral residence time. These two issues reduce krypton ionization probability and may account for some of the lowered performance relative to xenon. This is consistent with the krypton ion velocity distributions that show late ionization occurring throughout the acceleration channel and into the plume, thereby implicating reduced krypton propellant utilization as one of the most dramatic differences.

Significant resources have been expended to develop design rules for xenon Hall effect thrusters, but there is less knowledge on how these design rules vary with propellant. Recent experimental optimization of krypton performance in specialized Hall effect thrusters have shown performance improvements with optimized ionization/acceleration channel length, increased magnetic field, and increases in plasma density. Application of advanced diagnostics, such as LIF, provides fundamental insights into the propellant acceleration of these notoriously complex plasma discharges. In this case, we are able to show that in this non-optimized krypton operation, the late term ionization is indicative of poor propellant utilization. Studies like this that directly compare multiple propellants in a thruster are valuable as they provide insights into the fundamental physics of Hall effect thruster propellants that are masked by global measurements of performance, or perturbed by intrusive probe based measurements. It is clear that further LIF examination of plasma acceleration must be performed for

krypton propellant performance optimized cases. This will enable comparison of optimized cases of both propellants. Still, this first comparison of matched atomic flow rate, magnetic field, and acceleration potential provides a much needed baseline verification of previous hypotheses of differences in propellant optimization.

Acknowledgments

The authors would like to thank D. Roberts and R. Gregory for their assistance in setting up the test apparatus. In addition, G. Reed was instrumental in the design of the data acquisition system. Much thanks is also due to Dr. C. Larson and Dr. N. Gascon, who provided invaluable pathfinding with regard to krypton Hall effect thruster performance.

References

- ¹R. Jahn, *Physics of Electric Propulsion*. McGraw-Hill, 1968.
- ²D. R. Lide, *Handbook of Chemistry and Physics*, 79th ed. CRC Press, 1998.
- ³O. Duchemin, D. Valentian, and N. Cornu, "Cryostorage of propellants for electric propulsion," in *Proceedings of the 45th Joint Propulsion Conference and Exhibit*, no. AIAA-2009-4912. American Institute of Aeronautics and Astronautics, August 2009.
- ⁴W. A. Hargus Jr. and M. A. Cappelli, "Laser-induced fluorescence measurements of velocity within a Hall discharge," *Applied Physics B*, vol. 72, no. 8, pp. 961–969, June 2001.
- ⁵W. A. Hargus and C. S. Charles, "Near exit plane velocity field of a 200 W Hall thruster," *Journal of Propulsion and Power*, vol. 24, no. 1, pp. 127–133, January-February 2008.
- ⁶S. Mazouffre, D. Gawron, V. Kulaev, and N. Sadeghi, "A laser spectroscopic study on Xe^+ ion transport phenomena in a 5 kW-class Hall effect thruster," in *Proceedings of the 30th International Electric Propulsion Conference*, no. IEPC-2007-160. Florence, Italy: Electric Rocket Society, September 2007.
- ⁷M. R. Nakles and W. A. Hargus Jr., "Background pressure effects on internal and near-field ion velocity distribution of the BHT-600 Hall thruster," in *Proceedings of the 44th Joint Propulsion Conference and Exhibit*, no. AIAA-2008-5101. Hartford, CT: American Institute of Aeronautics and Astronautics, July 2008.
- ⁸W. A. Hargus Jr., M. R. Nakles, B. Pote, and R. Tedrake, "The effect of thruster oscillations on axial velocity distributions," in *Proceedings of the 44th Joint Propulsion Conference and Exhibit*, no. AIAA-2008-4724. Hartford, CT: American Institute of Aeronautics and Astronautics, July 2008.
- ⁹T. Fujimoto and A. Iwamae, Eds., *Plasma Polarization Spectroscopy*, ser. Series on Atomic, Optical and Plasma Physics. Springer-Verlag, 2008, vol. 44.
- ¹⁰W. Demtroder, *Laser Spectroscopy: Basic Concepts and Instrumentation*. Springer-Verlag, 1996.
- ¹¹W. A. Hargus, "A preliminary study of krypton laser-induced fluorescence," in *Proceedings of the 46th Joint Propulsion Conference and Exhibit*, no. AIAA-2010-6524. American Institute of Aeronautics and Astronautics, August 2010.
- ¹²W. A. Hargus, G. M. Azarnia, and M. R. Nakles, "Kr II laser-induced fluorescence for measuring plasma acceleration," *Review of Scientific Instruments*, vol. 83, no. 103111, 2012.
- ¹³W. A. Hargus and M. R. Nakles, "Ion velocity measurements within the acceleration channel of low-power Hall thruster," *IEEE Transactions on Plasma Science*, vol. 36, no. 5, pp. 1989–1997, October 2008.
- ¹⁴M. R. Nakles and W. A. Hargus, "Background pressure effects on ion velocity distribution within a medium-power Hall thruster," *AIAA Journal of Propulsion and Power*, vol. 27, no. 4, pp. 737–743, July-August 2011.
- ¹⁵M. R. Nakles, R. R. Barry, C. W. Larson, and W. A. Hargus, "A plume comparison of xenon and krypton propellant on a 600 W Hall thruster," in *Proceedings of the 31st International Electric Propulsion Conference*, no. IEPC-2009-118, Ann Arbor, MI, September 2009.
- ¹⁶I. Leybold-Heraeus Vacuum Products, *Vacuum Technology its Foundations Formulae and Tables*. Leybold-Heraeus Vacuum Products, Inc., 1987.
- ¹⁷B. Barbieri, N. Beverini, and A. Sasso, "Optogalvanic spectroscopy," *Review of Modern Physics*, vol. 62, no. 3, pp. 603–644, July 1990.
- ¹⁸H. Geisen, T. Krumpelmann, D. Neuschafer, and C. Ottinger, "Hyperfine splitting measurements on the 6265 angstrom and 6507 angstrom lines of seven Xe isotopes by LIF on a beam of metastable $\text{Xe}(3p0,3)$ atoms," *Physics Letters A*, vol. 130, no. 4-5, pp. 299–309, July 1988.
- ¹⁹W. Fischer, H. Huhnermann, G. Kromer, and H. J. Schafer, "Isotope shifts in the atomic spectrum of xenon and nuclear deformation effects," *Z. Physik*, vol. 270, no. 2, pp. 113–120, January 1974.
- ²⁰L. Bronstrom, A. Kastberg, J. Lidberg, and S. Mannervik, "Hyperfine-structure measurements in Xe II," *Physical Review A*, vol. 53, no. 1, pp. 109–112, January 1996.
- ²¹D. H. Manzella, "Stationary plasma thruster ion velocity distribution," in *Proceedings of the 30th Joint Propulsion Conference and Exhibit*, no. AIAA-1994-3141. American Institute of Aeronautics and Astronautics, June 1994.
- ²²J. E. Hansen and W. Persson, "Revised analysis of singly ionized xenon, Xe II," *Physica Scripta*, no. 4, pp. 602–643, 1987.
- ²³M. H. Miller and R. A. Roig, "Transition probabilities of Xe I and Xe II," *Physical Review A*, vol. 8, no. 1, pp. 480–486, July 1973.
- ²⁴C. E. Moore, *Atomic Energy Levels*. National Bureau of Standards, 1958, vol. II.
- ²⁵W. A. Hargus, G. M. Azarnia, and M. R. Nakles, "Demonstration of laser-induced fluorescence on a krypton Hall effect thruster," in *Proceedings of the 32nd International Electric Propulsion Conference*, no. IEPC-2011-018. Electric Rocket Society, September 2011.
- ²⁶W. A. Hargus Jr. and M. R. Nakles, "Evolution of the ion velocity distribution in the near field of the BHT-200-x3 Hall thruster," in *Proceedings of the 42nd Joint Propulsion Conference and Exhibit*, no. AIAA-2006-4991. Sacramento, CA: American Institute of Aeronautics and Astronautics, July 2006.
- ²⁷E. Y. Choueriri, "Plasma oscillations in Hall thrusters," *Physics of Plasmas*, vol. 8, no. 4, pp. 1411–1426, April 2001.
- ²⁸S. Yoshikawa and D. J. Rose, "Anomalous diffusion of a plasma across a magnetic field," *Physics of Fluids*, vol. 5, no. 3, March 1963.
- ²⁹A. I. Bugrova, A. S. Lipatov, A. I. Morozov, and L. V. Solomtina, "Global characteristics of an aton stationary plasma thruster operating with krypton and xenon," *Plasma Physics Reports (Trans. Fizika Plazmy)*, vol. 28, no. 12, pp. 1032–1037, 2002.
- ³⁰A. I. Bugrova, A. S. Lipatov, A. I. Morozov, and D. V. Churbanov, "On a similarity criterion for plasma accelerators of the stationary plasma type," *Technical Physics Letters (Trans. Pis'ma v Zhurnal Tekhnicheskoi Fiziki)*, vol. 28, no. 10, pp. 821–823, 2002.
- ³¹A. I. Bugrova, A. M. Bishaev, A. V. Desyatskov, M. V. K. adn A. S. Lipatov, and M. Dudeck, "Experimental investigations of a krypton stationary plasma thruster," *International Journal of Aerospace Engineering*, vol. 2013, no. 686132, 2013.